Hydrogen Welding and Hydrogen Switches in a Mono-Atomic Gold Nanowire

*Robert N. Barnett, Hannu Häkkinen, Andrew G. Scherbakov, and Uzi Landman**

School of Physics, Georgia Institute of Technology, Atlanta, GA 30332

Abstract

Ab-initio density-functional calculations are performed to study the interaction between a mono-atomic gold nanowire suspended between two gold tips and hydrogen, in the molecular, quasi-dissociated, dissociated and atomic forms. Structural configurations, electronic states, vibrational modes, and electronic transport are investigated for several elongation stages of the wire, corresponding to the last conductance plateau ($G \approx 1g_0$, $g_0 = 2e^2 / h$) before breaking of the contact. We illustrate "welding" and restoration of electric conductance of a broken wire through the incorporation of an H_2 molecule, and an electric switching action resulting from structural fluctuations of an adsorbed molecule caused by mechanical forces applied to the wire.

* Corresponding author: email uzi.landman@physics.gatech.edu

Formation, stability, structural, and mechanical characteristics of nanowires (NWs) formed upon separation of the contact between a tip and a surface have been predicted in early simulations[1], and these properties, as well as the electronic structure and electric transport in metal NWs, have been the subject of subsequent significant research efforts[2]. These endeavors were motivated by fundamental interest in the properties of materials contacts and wires in the nanoscale regime, as well as by prospects of using stable electrical contacts of nanoscale dimensions in future nanoelectronics.

The ultimate limit of a thin conductor is a nanowire composed of an atomic chain. Such NWs have indeed been observed in the aforementioned early simulations of gold nanowires[1], as well as in the first *ab-initio* simulations of sodium nanowires[3], and more recently they have been imaged by high-resolution transmission electron microscopy (HRTEM) as a gold STM tip was retracted from gold surface[4]. Formation of atomic gold chains comprised of several atoms has also been reported in break-junction experiments[5], and imaged via HRTEM as connecting bridges between areas in thin gold films perforated by impact of energetic electrons [4, 6]. In addition to these experimental studies the atomic and electronic structure, as well as electric conductance in such monoatomic NWs, have been the focus of several theoretical investigations [7-12].

While to date, investigations of nanowires focused mainly on clean (bare) systems, it is natural to enquire about modifications of the mechanical, structural, and electronic properties of NWs that may be brought about as a result of their interactions with atomic and molecular species. Such issues may be pursued from both fundamental and applied perspectives. In particular, we remark here on “nanowire chemistry” that may be viewed as an emerging topic in the broader field of nanocatalysis[13,14] which aims at investigations of the chemical properties and catalytic activity of systems where at least one of the dimensions has been reduced to the nanoscale. Indeed, understanding the nature of such chemical interactions may provide new avenues for chemical sensing and for catalytic applications. In the context of nanocatalysis we remark that recent research in this area focused on nanoscale gold structures, which have been found (experimentally and theoretically) to exhibit unique chemical and catalytic properties. These remarkable chemical properties of gold, which in it's bulk form is known to be chemically inert, have been shown to originate from the strongly modified electronic structure of gold nanoclusters and nanostructures as their size and/or dimensionality are reduced.[13,14,15]

Currently investigations of nanowires interacting with atomic or molecular species are rather scarce. Examples include: (i) Measurements of the electronic transport properties of nanowires in solution, prepared in an electrochemical cell [16, 17, 18]; (ii) an early theoretical (density-functional) investigation of structural, electronic and transport effects of molecular adsorption on the properties of a nanowire[10] - in particular, bonding of methyl thiol to a monoatomic gold nanowire – with implications pertaining to "anomalously" large inter-gold distances reported in some HRTEM measurements [4,6]; in this study[10] it was first suggested that the above anomaly has it's origins in the increased distance between neighboring gold atoms caused by interactions with a light chemical species (e.g. sulfur, carbon, hydrogen) – since the latter is essentially invisible under the imaging conditions used for viewing the gold it's undetected presence can lead to the (erroneous) assignment of an unusually large inter-gold distance; (iii) more recent theoretical investigations of the interactions of various elements (e.g, hydrogen, carbon , sulfur atoms), focusing on the above – mentioned "distance anomaly" [19, 20, 21]; and (iv) most recent experimental and theoretical investigations of the interaction of hydrogen with platinum and gold wires.[22, 23, 24]

In this communication we report an extensive density-functional investigation on the interaction of hydrogen with an atomic gold wire suspended between gold tips. We demonstrate a novel mechanism for the H_2 – wire interaction where the hydrogen molecule can adsorb on the wire either dissociatively or molecularly depending on the stretching state of the wire. The dissociative adsorption, which is stabilized by relativistic bonding effects in gold, "switches off" the conductance of the wire, while the molecular "bridging" adsorption induces an increase in the conductance of the highly strained wire and can even restore a (fractional) conductance in a broken gold contact, with the hydrogen molecule acting as a "welding" agent. We also discuss vibrational modes of adsorbed molecular hydrogen, and illustrate their sensitivity to the elongation of the nanowire.

Computational method. The calculations were performed using the ab-initio Born-Oppenheimer (BO) local-spin-density (LSD) molecular dynamics method (BO-LSD-MD)[25] including self-consistent gradient corrections (GGA)[26] to the exchange-correlation functional. The $5d^{10}6s^1$ valence electrons of a gold atom are described by scalar-relativistic norm-conserving nonlocal pseudopotentials[27] (core radii: $s(2.5\ a_0)$, $p(3.0\ a_0)$, $d(2.0\ a_0)$, with s as the local component) using a plane-wave basis set with a kinetic energy cutoff of 62 Ry. For hydrogen, an s-only local pseudopotential with a core radius of $0.95\ a_0$ was used.

In calculations of the conductance we used a recursion-transfer-matrix method[28]. In this method the transmission of an electron propagating from one electrode to the other through the GGA self-consistent effective potential[29].of the connected nanowire, calculated for each of the relaxed wire configurations and processed according to the procedure described in ref.. 30, is evaluated using a numerical solution for the stationary states to the Schrodinger equation with scattering boundary conditions. Inside the electrodes, i.e., away from the wire/electrode contact region the effective potential converges to a constant "jellium" value which is then used to represent the continuation of the electrodes. The solution is achieved via discretization of the Schrodinger equation in slices along the wire axis and using periodic boundary conditions in the transverse directions. Transfer-matrix recursion formalism is used to propagate the solution from one slice to the adjacent one starting from the constant-potential region in one of the electrodes and propagating through the wire into the constant-potential region of the receiving electrode. In these conductance calculations 512 plane waves were used to achieve convergence. Transformation to non-mixing eigenchannels was performed following ref.. 31. The recursion-transfer-matrix method as currently implemented requires a local potential, so in the conductance calculations we treated Au as a $6s^1$ valence electron atom and have solved self-consistently to get the local potential to use in the conductance calculations. This procedure is supported by the close resemblance of the local density-of-states and of the wavefunctions on the wire atoms near the Fermi level compared to the results for the full $5d^{10}6s^1$ valence eletrons solution.

Au-wire setup. Figure 1 shows the setup used in our simulations and Table I gives the basic parameters (L, $d_{aa'}$, $d_{bb'}$, d_{ab}, d_{bc}) defining the bare Au-wire (B-wire) and the additional ones (α, $d_{H-H'}$, d_{a-H}) with the wire interacting with an H_2 molecule (H_2-wire), or with a single hydrogen atom (H-wire). The parameter L gives the distance between the two outermost atomic layers of the two opposing supporting tips (with the atoms in these two layers treated statically, while all other atoms are allowed to relax. dynamically after each elongation stage, i.e., when L is varied). The actual length of the mono-atomic wire is given by $L_w \equiv d_{bb'}$.

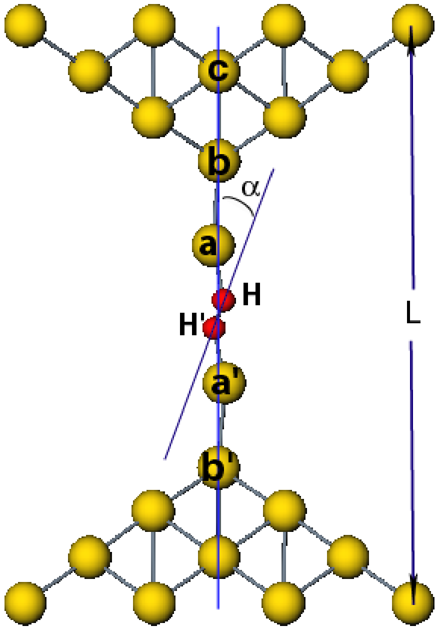

Figure 1: The wire setup used in the calculations; see the caption to Table I for the definitions of the geometric parameters.

Table 1. Geometry, energetics, and conductance of the wires.

label [a]	L [b]	ΔE [c]	F_s (nN) [d]	BE(H2) [e]	G (g_0) [f]	$d_{b\text{-}b'}$ [g]	$d_{a\text{-}a'}$ [g]	$d_{a\text{-}H}$ [g]	α [h]	$d_{H\text{-}H'}$ [g]	$d_{a\text{-}b}$ [g]	$d_{b\text{-}c}$ [g]
Bare Wires :												
(i)	16.25	-1.24	-0.4		0.91	7.89	2.61				2.64	2.74
(ii)	17.25	-0.74	-1.4		0.87	8.51	2.79				2.86	2.93
(iii)	17.75	-0.37	-1.2		0.54	8.99	2.71				3.14	2.93
(iv md)	18.00	-0.10	-0.6		0.72	9.41	2.68				3.36	2.88
(iv ed)	18.00	-0.11	-0.1		0.05	9.44	4.19				2.62	2.89
(v)	18.25	-0.05	0.2		0.02	9.71	4.49				2.61	2.83
(vi)	18.40	-0.05	0.1		0.01	9.91	4.73				2.59	2.81
Wires with H_2 molecule :												
(vii)	16.25	-1.21	0.1	0.06	0.11	7.94	2.80	1.73	90	2.02	2.57	2.72
(viii)	17.25	-0.98	-1.2	0.32	0.07	8.51	3.05	1.75	90	1.74	2.73	2.93
(ix)	17.75	-0.77	-0.5	0.48	0.21	9.23	3.93	1.75	53	0.94	2.65	2.83
(x)	18.00	-0.78	-0.1	0.77	0.24	9.46	4.15	1.75	37	0.93	2.66	2.83
(xi)	18.25	-0.68	-0.1	0.70	0.25	9.72	4.36	1.76	19	0.94	2.68	2.84
(xii)	18.40	-0.61	-0.4	0.63	0.23	9.86	4.50	1.79	0	0.92	2.68	2.83
(xiii)	19.00	-0.30	-1.4	0.38	0.13	10.34	4.98	2.07	0	0.83	2.68	2.88
(xiv)	19.40	-0.12	-1.1	0.20	0.05	10.86	5.62	2.53	0	0.78	2.62	2.83
								($d_{a'H'}$=2.31)				
Broken wire:		0.00	0.0	0.08	0.00	>11.2	> 6.00	2.03	0	0.78	2.60	2.81
Wires with dissociated 2H :												
(xv)	17.25	-1.54	-1.1	0.88	0.06	8.56	2.74	1.72	0	5.62	2.91	2.91
(xvi)	18.25	-0.84	-0.2	0.88	0.09	9.63	2.71	1.72	0	6.16	3.46	2.86
(xvii)	18.40	-0.79	-0.4	0.82	0.01	9.77	2.79	1.73	0	6.26	3.49	2.87
Wire with weakly bound H2 molecule :												
(xviii)	17.25	-0.70	-0.4	0.05	0.22	8.78	3.54	1.66	16	1.01	2.62	2.79
Wire with a single H :												
(xix)	17.08		-0.6		0.00	8.54	3.37	1.69			2.59	2.82

[a] Labels *(i), (ii),* etc identify the wire configuration and correspond to those of Figs. 2 and 3, and throughout the text. [b] Distance (Å) between the outermost (base) atomic layers (see Fig. 1). [c] Energy difference (eV) from a completely separated tip configuration (broken, with H_2 adsorbed to one tip if present). [d] Force of constraint (nN=0.62eV/ Å) applied to the base layers (F_s<0 means the wire is under tension). [e] Energy difference (eV) from bare wire (same L) plus H_2 molecule. [f] Conductance (g_0=$2e^2/h$). [g] Distance (Å) between the specified atoms (see Fig. 1). For reference we note that for the isolated hydrogen molecule $d_{H\text{-}H'}$ = 0.75 Å and H_2 binding energy is 4.5 eV.

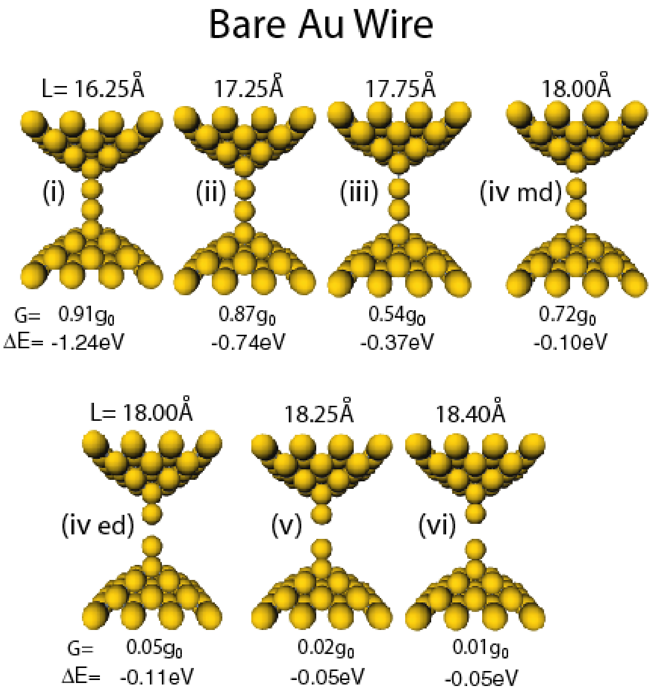

Figure 2: Optimal configurations of bare wires. The labels *(i), (ii),* etc. correspond to the first column of Table 1. For L = 18.00 Å two nearly degenerate configurations are shown - with a middle-dimer (iv md) and end-dimer (iv ed) structures. For each configuration we also give the conductance (G), and the total energy difference (ΔE) between the given configuration and the two separated tips.

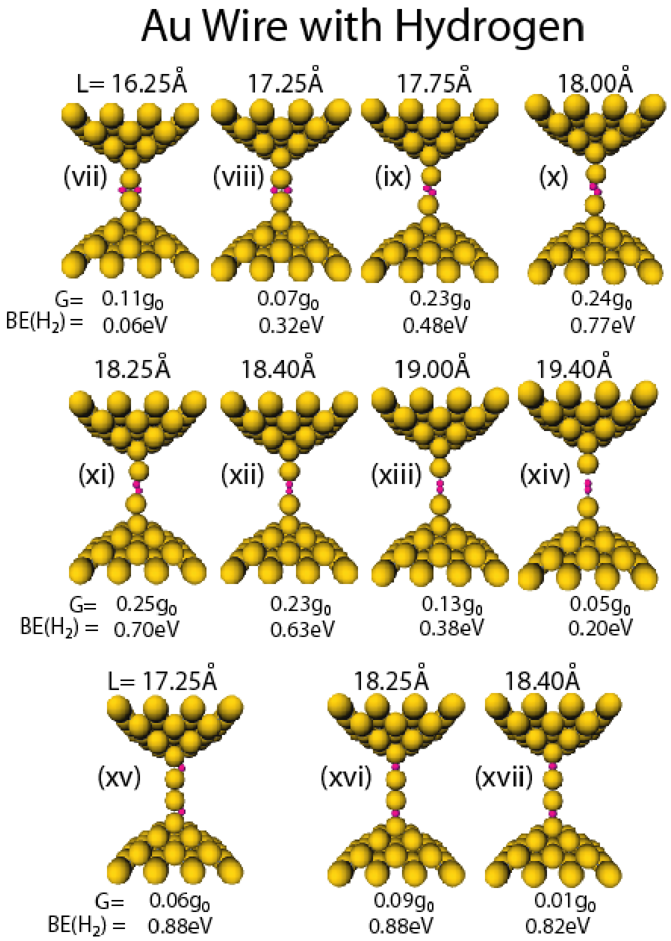

Figure 3: Gold wires with adsorbed hydrogen (small red spheres). Configurations (vii) and (viii) are quasi-dissociated; for larger L the adsorbed hydrogen molecules exhibit an increasing tilt angle with respect to the wire axis; (xiv) corresponds to an essentially broken wire. Hydrid-wire configurations are shown in the bottom row. G is the conductance, and BE(H_2) is the energy difference between the given configuration and the bare wire plus H_2 molecule.

Some of the B-wire relaxed configurations that we have studied are displayed in Fig. 2, and in Fig. 3 we show relaxed configurations of the wire with hydrogen adsorbed. We remark that a similar setup for the bare Au wire has been used by us in a previous study of the formation mechanism of single-stranded wires from an initial double-stranded contact.[12] The wire system is studied here at several selected values of the stretching parameter L in the range of 16.25 Å ≤ L ≤ 19.41 Å. The chosen lower limit of L=16.25 Å corresponds to the onset of the linear mono-atomic wire found by us earlier for this system (for L < 16.25 Å, bent and zigzag configurations appear)[12]. For each L the four atoms in the wire and the first and second layer atoms in the tips are fully relaxed.

In addition to the geometric parameters which characterize the wires, we give in Figs. 2 and 3 the calculated electronic conductance (G), the energy difference with respect to the completely separated tips (ΔE in Fig.2) and the H_2 binding energy (BE(H_2) in Fig.3). These properties are also given in Table 1, and they are plotted versus elongation of the wire (ΔL with respect to the value L=16.25 Å mentioned above) in Fig. 4. Included also in Table 1 is the magnitude of the stretching force (F_S), calculated for each equilibrated configuration (with a selected value of L) as the force acting on the two outermost layers of the supporting tips – that is, F_S is the force required in order to maintain the given strain in the system.

Bare Wire. We discuss first certain properties of the bare gold wire. From inspection of Fig. 4 (bottom) and Table 1 we conclude that varying the distance between the opposing tips influences mainly interatomic distances in the mono-atomic wire region, with the length of the wire $L_w \equiv d_{bb'}$ increasing monotonically with ΔL. At L=18.00 Å (i.e. ΔL = 1.75 Å) the wire exhibits a structural bistability, with two energetically degenerate configurations occurring, a middle – dimer one (marked (iv md) in Fig.2) and an end – dimer one (marked (iv ed) in Fig.2). For larger elongations the ed configuration dominates, resulting eventually in “breakage” of the B-wire.

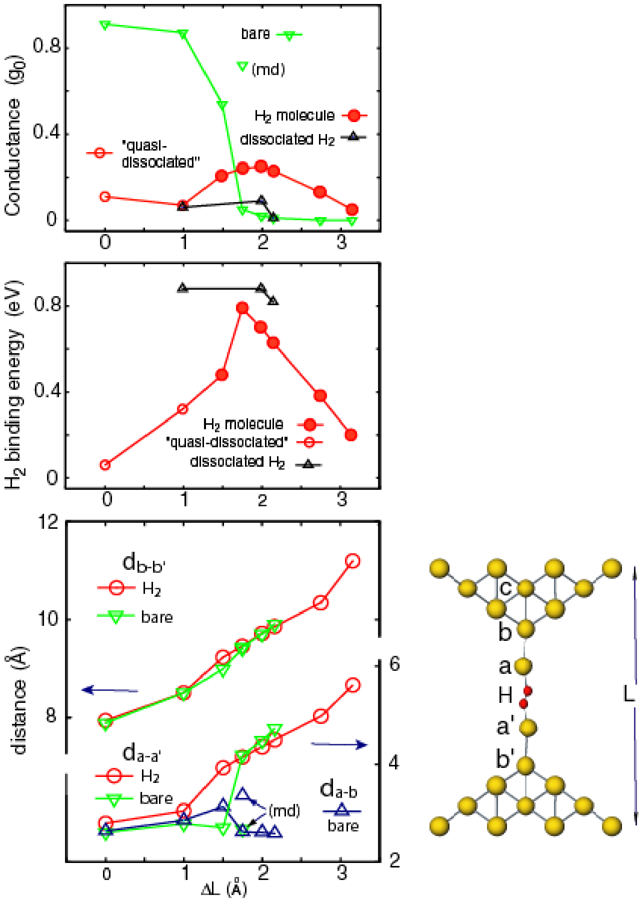

Figure 4: The conductance in units of g_0(top panel), the hydrogen binding energy BE(H_2) in eV (middle panel), and the variation of various distances (in Å), plotted versus the elongation $\Delta L = L - L_0$, $L_0 = 16.25$ Å (see also Table 1). The meaning of the various symbols is indicated in the figure. The "quasi-dissociated" configurations are those shown in the top row of Fig. 3 ((vii) and (viii)), and the dissociated configurations are those shown in the bottom row in Fig. 3 (i.e. the hydrid states, labeled (xv), (xvi) and (xvii)). For $\Delta L = 1.75$ Å we show (for the bare wire) in the top and bottom panels results for two nearly degenerate configurations – a "middle-dimer" (md) and an "end-dimer" (ed); only the md is marked.

The structural variations of the wire are portrayed in changes in the conductance of the bare wire that is influenced only slightly when $\Delta L = 1$ Å but drops in a step-like manner for larger elongations (see Fig.4 top panel); note that the aforementioned bistable configurations differ greatly in conductance, with the md configurations exhibiting a much higher conductance (0.72 g_0) then the ed one. From the electrical transport point of view the contact is essentially broken for $L \geq 18.25$ Å (see Figs. 2 and 4). We also note that at that for $L \geq 18.25$ Å the force required to maintain the given wire configuration changes sign; i.e. while for smaller values of L an "outward pointing" force was required in order to counterbalance the attraction between the two parts of the system, that attraction stops for $L \geq 18.25$ Å.

Insertion of H_2 into the broken Au contact – welded nanowire. Letting the aforementioned essentially broken Au wire (L= 18.25 Å, G = 0.02 g_0, marked (v) in Fig.2 and Table 1) interact with a hydrogen molecule results in a barrierless insertion of the molecule into the contact with a significant binding energy BE(H_2) = 0.70 eV ((xi) in Fig.3 and Table 1). Concomitantly, the conductance of the "welded" contact increases from close to zero to G = 0.25 g_0 indicating partial opening of one conductance channel; see our remark in ref. 23 pertaining to differences between the calculated conductance and that measured in experiments on physisorbed H_2 at 10-30K. At this value of L the H_2 molecule is slightly tipped and further stretching allows it to straighten. For L larger then 19.40 Å (L_w = 10.86 Å) the conductance essentially vanishes and the wire is finally broken.

A barrierless insertion of the H_2 molecule occurs also for L = 18.0 Å (recall the bistable B-wire mentioned above). Here the molecule is more strongly tilted with respect to the wire axis and the binding energy to the wire is peaked at 0.77eV (see Fig. 4, middle panel, and configuration (x) in Table 1). As seen in Figure 3(x) the adsorption of the hydrogen molecule is accompanied by stabilization of the "end–dimer –like" configuration, with a relatively high conductance G= 0.24 g_0 (see Fig. 4, top panel). Elongation of the wire for L > 18.25 Å (L_w > 9.72 Å, see Table 1) results in smaller binding energies of to the wire and decreasing conductance. We note that the incorporation of the hydrogen molecule in the wire allows the wire to extend to larger lengths then the bare Au wire (see in particular the bottom panel of Fig. 4).

When instead of elongating the wire, it is compressed (starting from the welded configuration at L= 18 Å) the tilt angle the adsorbed molecule increases and the binding energy to the wire decreases sharply (see Fig. 3, middle panel of Fig 4 and (ix) in Table 1). From the bottom panel of Fig. 4 we observe that the length of the wire $L_w \equiv d_{bb'}$ as a function of the elongation ΔL is the same for the bare wire and the one with the adsorbed hydrogen. This is due to the fact that the adsorption of the molecule results in rearrangement of the gold atoms in the internal part of the wire (see $d_{aa'}$ in the bottom panel of Fig.4), with the two end atoms that connect the wire to the two tips remaining at almost constant distance from the respective first (4-atom) layer of the supporting tip. Finally we remark that at a short distance L=17.25 Å we found that H_2 binds molecularly to the side of the wire (configuration (xviii) in Table 1, and in Fig. 7 below) with a binding energy BE (H_2) = 0.05 eV, and a conductance G = 0.22 g_0 that is a little less then half that of the corresponding B-wire (configuration (ii) in Table 1 and Fig.2). The barrier to remove the H_2 molecule starting from the latter equilibrium configuration reaches a maximum of about 0.4eV at a radial distance of 1.6 Å from the wire axis (determined by minimizing energy with constrained distance from the wire axis to the H_2 center of mass). The H_2 molecule did not bind to the side of shorter wires.

H_2 quasi-dissociation and the "hydrogen switch". Compression of the wire from L=18.25 Å to L=17.25, and further to16.25 Å, results in quasi-dissociation of the molecule, with the H-H axis perpendicular to the wire axis; d_{H-H} = 1.74 Å and BE(H_2) = 0.32 eV for L=17.25 Å and d_{H-H} = 2.02 Å and BE(H_2) = 0.06 eV for L=16.25 Å – see configurations (viii) and (vii) in Fig 3 and Table 1, respectively. The binding energies of the quasi-dissociated molecule to the wire in these compressed states are lower than the starting welded configuration (see middle panel in Fig. 4). While the quasi-dissociation of H_2 upon compression is barrierless, a rather high activation barrier is encountered (larger then 0.8 eV) for recombination of the H atoms and removal of the H_2 molecule from the wire at L=17.25 Å. This indicates that once the quasi-dissociated state of the molecule has been formed it is stable and subsequently it may lead to the appearance of "hydride states" (see below).

Bonding of H_2 to the Au-wire has been analyzed by projecting the electron local density of states (LDOS) onto the hydrogen atoms and the neighboring Au atoms on the wire axis (labeled in Fig. 1 as a, a', b, b',c). These LDOS are shown in Figure 5(a) and 5(b), respectively, for the quasi-dissociated molecule at L=17.25 Å (viii) and for the bridging-molecule case at L=18.4 Å (xii). We also include in Fig.5(c) the projected LDOS for a Au wire with an embedded single hydrogen atom (configuration (xix) in Table 1). In Fig. 6 we display isosurfaces corresponding to several wavefunctions near the Fermi level for the three systems shown in Fig. 5.

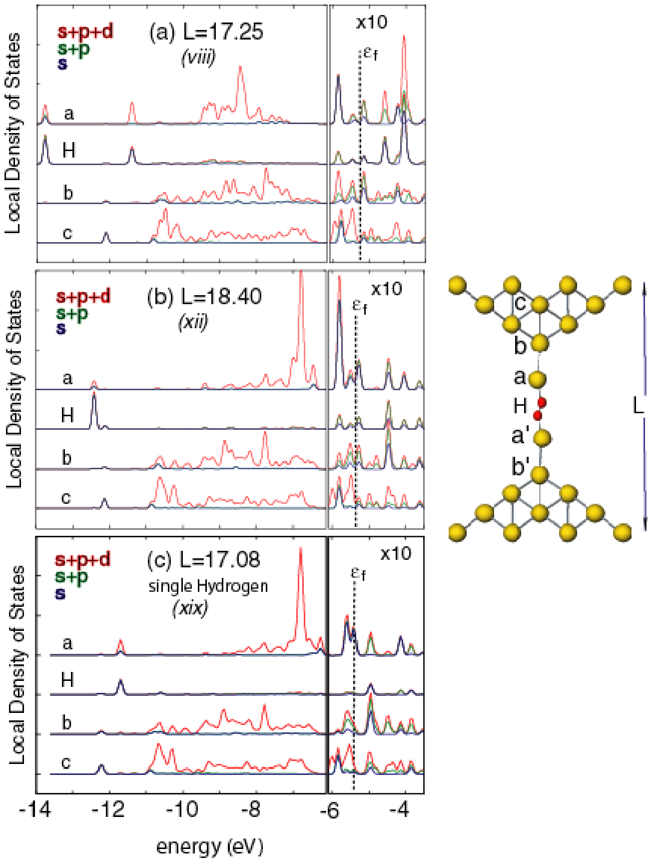

Figure 5: The local density of states (LDOS) for the optimal configurations of a gold nanowire with adsorbed hydrogen, corresponding to (a) L = 17.25 Å (a quasi-dissociated molecule), and (b) L = 18.40 Å (a hydrogen molecule inserted into the wire). The LDOS for a gold wire with an adsorbed single hydrogen atom is shown in (c). These LDOS plots were calculated using a sphere of radius 1.6 Å centered on the Au atoms (labeled a, b and c, see Fig 1) or of radius 1.3 Å centered on the H atoms. The LDOS is decomposed into s, p, and d components: the blue curve is the s component, the green is the sum of s and p components, and the red is the sum of s, p, and d components. There is a gap below about –6.2eV, and the LDOS for energy above this gap is shown multiplied by a factor of 10.

For the bridging-molecule (Fig. 5(b), only one major peak in the LDOS of the hydrogen atoms is seen (located at –12.4 eV in fig. 5b) and it corresponds to the lowest occupied molecular orbital (LOMO, see Fig. 6) of the entire system (tips, wire and hydrogens), located about 7 eV below the Fermi energy E_F. This state is found to be a superposition of the $\sigma(H_2)$ bonding molecular orbital and the 5d(m=0) states of the Au atoms of the wire axis, creating a bonding state that extends along the wire axis. The antibonding state of the bridging molecule is unoccupied and it lies outside the enrgy interval shown in the figure.

For the quasi-dissociated molecule (Fig. 5a) in addition to the LOMO state (located at about –13.9 eV) another state is found below the gold d-band that has a large amplitude on the H atoms (marked as LOMO+3 in Fig. 6(a), with an energy of about –11.7 eV). This state corresponds to the anti-bonding $\sigma^*(H_2)$ orbital that is mixed with the Au 5d states. We note that in both cases the highest occupied state (HOMO in 6(a,b)) and lowest unoccupied (LUMO in Fig. 6(a,b)) are delocalized over the entire system, with the LUMO showing features of the bonding σ(H_2) state, and the HOMO showing features of the antibonding σ*(H_2) state, and both are hybridized with the 6s-state of the neighboring Au atoms in the wire region (the atoms labeled (a and a') in Fig. 1). We also note here that for the single adsorbed hydrogen atom the hydrogen 1s orbital hybridizes with a 5d orbital of the neighboring gold atom (see the state at –11.6 eV in Fig. 5(c)). We note however that the LDOS on the hydrogen atom vanishes at the Fermi level, and the LUMO orbital has no amplitude on the wire atoms and the hydrogen atom (see Fig.6 bottom row).

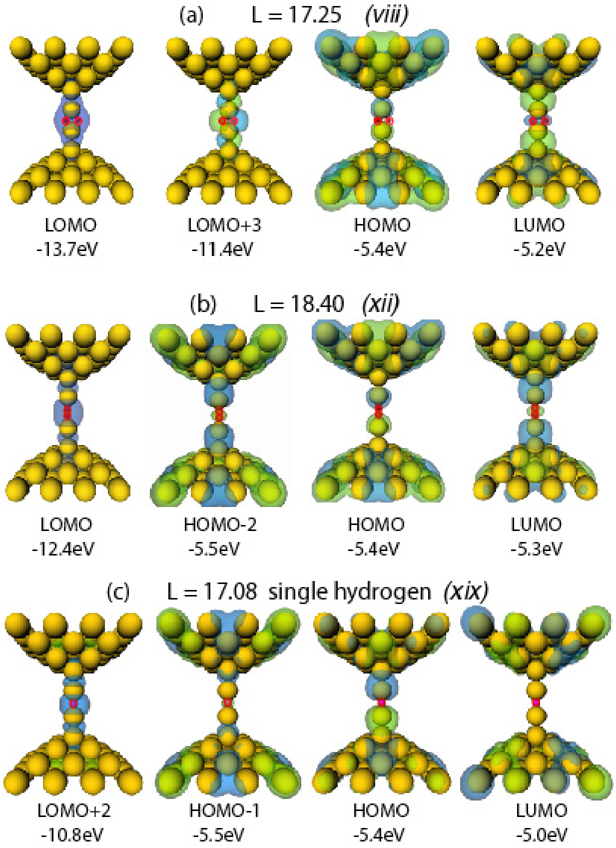

Figure 6: Wavefunction iso-surfaces for the quasi-dissociated (a) and bridging-molecule (b) cases, configurations (viii) and (xii), respectively, in of Fig.3 and Table 1. The LDOS for a wire with single adsorbed hydrogen aton (configuration (xix) in Table 1) is shown in (c). In these plots, LOMO is the "lowest-occupied" state, which is predominately the H_2 binding orbital in case (a) and (b). HOMO and LUMO are the "highest-occupied" and "lowest-unoccupied" states. Also shown are the "LOMO+3" wavefunction for the quasi-dissociated case(a), which is largely the H_2 anti-bonding orbital (a similar state is not found for the bridging-molecule configuration since the antibonding state lies above the energy interval shown here), and the "HOMO-2" for the bridging-molecule case shown in (b) (corresponding to the large peak in the LDOS of the Au atoms adjacent to the H_2). The iso-surfaces include 95% of the orbital; the green and blue correspond to positive and negative values, separated by nodal surfaces.

The fact that the H_2 molecule interacts so strongly with the gold wire is quite surprising in light of the well documented inertness of gold surfaces toward adsorption and/or promotion of dissociative H_2 adsorption. However, early experiments of the reactions of neutral gas-phase coinage metal dimers indicated that among Cu_2, Ag_2, and Au_2, the gold dimer is the only one that interacts with H_2; additionally, these experiments indicated a slow pressure-independent rate constant and insertion of gold into the H-H bond [32].

To further investigate these points, we performed comparative calculations for a free linear four-atom cluster Au_4 with H_2 adsorbed in the middle and found that depending on the nature of the gold pseudopotential (scalar-relativistic (SR) or non-relativistic (NR)) the interaction energy is either binding (by 1.07 eV) for the SR Au_4 or non-binding (by 2.07 eV) for the NR gold quadramere cluster. Analysis of the local density of electronic states projected on the H atom reveals that the tendency for the SR Au_4 wire to dissociatively bind H_2 is due to the strong bonding overlap of the antibonding $\sigma^*(H_2)$ state with one of the d(m=±1, Au) states. As a result of the promotion of charge to the anti-bonding H_2 σ^* state the $\varepsilon(\sigma^*) - \varepsilon(\sigma)$ energy gap is only about 2.5 eV, whereas in the free H_2 molecule it is calculated to have a fourfold larger value of 10.2 eV. A similar scenario is observed for the suspended H_2 – wire with L = 16.25 Å and L = 17.25 Å – see Fig.5 for the LDOS and Fig. 6 for the corresponding wavefunctions' portraits, with the bonding LOMO, $\sigma(H_2)$, and the anti-bonding (LOMO+3), $\sigma^*(H_2)$, found to be localized in the four-atom region between the tips. To our knowledge this is the first time that the tendency of an Au wire to promote dissociative adsorption of H_2 is predicted and correlated to the relativistic bonding effects in gold.

The states of the wire with the adsorbed quasi-dissociated H_2 molecules exhibit highly reduced conductances compared to those of the corresponding bare wire configurations (Table 1, Fig. 4); at both L=17.25 Å and 16.25 Å the decrease is about 0.8 g_0. Isosurfaces of the calculated conductance eigen-channels (i.e. the vectors that diagonalize the transmission matrix, expressing the probability density for transmission) of several of the B- and H_2-wires (both conducting and nonconducting), are shown in Fig. 7. We observe that while for the B-wire ((ii) for L=17.25 Å in Fig.7) the conductance eigenchannel is spread rather uniformly over the entire system (tips and connecting nanowire constriction), the hydrogen atoms in the H_2-wire induce backscattering regions (regions with near vanishing probability density for transmission) for electrons in both of the tips and between the Au atoms in the wire marked (a) and the guest hydrogen atoms. This surprising theoretical prediction of the "hydrogen switch" effect could in principle be tested in well-controlled tip-surface experiments in hydrogen atmosphere.

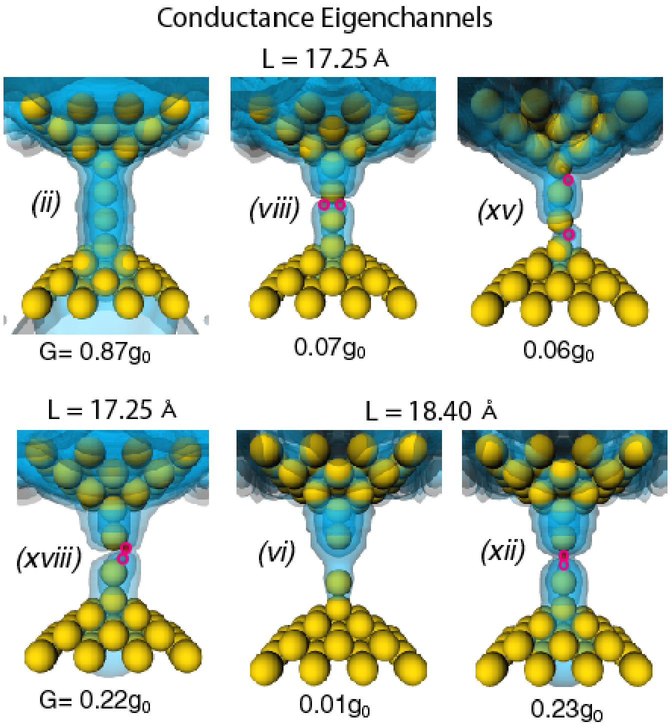

Figure7: Iso-surfaces of the Conductance eigenchannel density for several of the wire configurations. For L= 17.25 Å we display results for the bare wire (ii) the quasi-dissociated state (viii), the hydrid state (xv) and the weakly bound state (xviii). For L=18.40 Å we display results for the bare wire (vi) and the welded one (xii). The three nested isosurfaces correspond to 10%, 1%, and 0.1%.

Dynamical characteristics of the H_2-bridged gold contact. The adsorbed H_2 in the Au-wire remains molecular within the stretch region of $18.25 \leq L \leq 19.40$ Å (for larger values of L the wire is considered broken), with a maximum of H_2 binding energy and conductance (0.70 eV and 0.25 g_0, respectively) at L=18.25 Å. The dynamical properties of the H_2-bridged contact can be characterized by three H_2 vibration modes: a “shuttle motion” (vibration of the center of mass of the molecule along the Au-wire axis) with a frequency ω_1, a “wobble motion” (variations of the angle α) with a frequency ω_2, and the H-H bond stretch characterized by ω_3. We have determined the frequencies of these normal modes by *ab – initio* molecular dynamics simulations at three stretching states with L=17.25 Å, L=18.40 Å and 19.00 Å (see Fig. 8). At L=17.25 Å, $h\omega_1$=148 meV, $h\omega_2$=104 meV and $h\omega_3$=205 meV. At L=18.40 Å, $h\omega_1$=130 meV, $h\omega_2$=58 meV and $h\omega_3$=308 meV. At L=19.0 Å $h\omega_1$ decreases strongly to 64 meV, $h\omega_2$=71 meV and $h\omega_3$ is slightly reduced to 292 meV. We note here that recent scanning tunneling spectroscopy (STS) measurements, performed for a break-junction Pt atomic contact in H_2 atmosphere, yielded a typical resonance frequency of about 60 meV which was attributed to the “shuttle” motion of a bridging H_2 molecule across the Pt atom contact[22]. Our results illustrate the marked sensitivity of the vibrational frequencies of the molecule on the stretching state of the wire. Furthermore, we observe that, depending on the state of elongation, either a “wobble” motion of the molecule (see L= 18.40 Å in Fig. 8) or both a “shuttle” and “wobble” vibrations (see L=19.00 Å in Fig. 8) may contribute to the observation of a phonon frequencies close to 60 meV; in this context see our remark in ref 22.

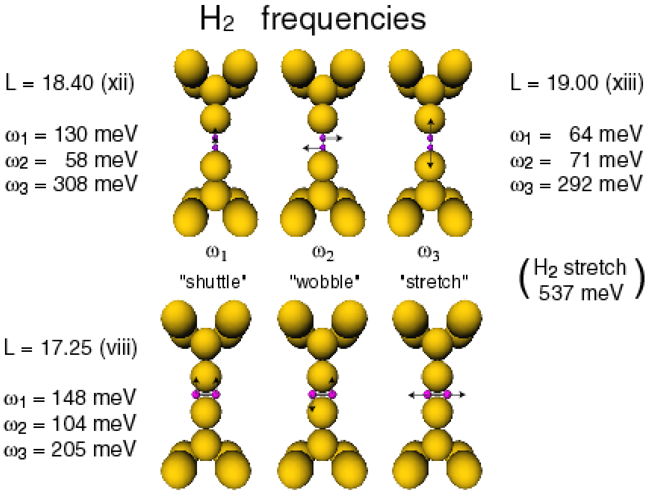

Figure 8: Vibrational modes of a hydrogen molecule adsorbed to a gold mono-atomic wire suspended between two supporting tips, calculated for different values of the inter-tip distance. The displacement vectors of the hydrogens corresponding to the various modes (shuttle, wobble and stretch vibrations) are shown for L=18.40 Å and L=17.25 Å; The displacement vector for the configuration with L=19.00 Å have the same character as those shown for L=18.40 Å.

Gold-hydride wire. As indicated above, the dissociation of the H_2 molecule inside the wire may lead to other arrangements of Au and H atoms, such as the ones depicted in Fig. 3 (xv) – (xvii). These "hydride" wires, characterized by linear or "zigzag" alternating -Au-H-Au- chains, could be formed for example by H atom diffusion after the dissociation of an H_2 molecule, or via diffusion from the tips to the wire region. We have not studied these mechanisms (and the barriers involved) in more detail, but we note here that the hydride wires are remarkably stable, in agreement with a recent computational study [24] (in fact, their total energies are the lowest ones in the stretching region of 17.25 Å ≤ L ≤18.4 Å, see Table 1). However, we find that the calculated conductance properties of the hydride wires are remarkably different from what was conjectured previously: while in ref. 21 an estimate of $G \approx 1$ g_0 was made on the basis of the calculated band structure of an infinite –Au-H-Au-H- wire, our explicit calculations on the transmission properties through the hydride wire and the tip regions indicate that the hydrogen atoms generate a significant backscattering of the electrons, and $G < 0.1$ g_0 for all the cases that we studied here (L=17.25 Å, 18.25 Å, and 18.4 Å). The eigenchannel for the hydride wire at L=17.25 Å is shown in Fig. 7 (xv). We also tried a single H between the two center gold atoms of an L=17.08 Å wire, and found the conductance to be zero.

Summary. In this study we explored through extensive electronic structure calculations based on density-functional theory, the energetics, structures, electronic states, and electrical conductance of: (i) bare gold nanowires made of a monoatomic chain suspended between two supporting tips, and (ii) these wires interacting with hydrogen. Our calculations revealed that the interaction between a hydrogen molecule and a suspended mono-atomic gold wire, and the optimal outcome of such interaction, exhibit a strong dependence on the elongation stage of the wire (occurring as a result of the displacement of the tips with respect to each other, thus straining the wire), and in some cases the interacting system may evolve along several alternative pathways.

The processes that we explored include: (i) "molecular welding" – where a hydrogen molecule adsorbs to the wire, forming a fractionally conducting bridge across a broken gold contact, (ii) barrierless quasi-dissociation of a hydrogen molecule occurring upon compression of the contact from the molecular welding configuration, accompanied by switching off of the wire conductance, and (iii) formation of a stable non-conducting gold-hydride wire as a result of the diffusion of hydrogen atoms following the afore-mentioned quasi-dissociation of the molecule, or as a consequence of diffusion of atomic hydrogen from the tips to the wire region. In addition to the structural and electric transport properties of the bare and hydrogen-adsorbed nanowire configurations we investigated the dynamical characteristics of the adsorbed hydrogen molecule, and have illustrated the sensitivity of the various vibrational modes to the elongation state of the wire.

The various adsorption states of hydrogen to suspended mono-atomic gold wires revealed by our investigations, and their structural, transport and dynamical properties, should prove useful for understanding the stability and conductance of atomic gold contacts in a hydrogen atmosphere, and for the interpretation and elucidation of experiments under such conditions. Finally, we note that the reactivity of gold nanowires with hydrogen (in contrast to the well accepted inertness of bulk gold) is consistent with recent findings pertaining to the chemical catalytic activity of gold nano-clusters (in the gas phase and when supported on metal-oxide surfaces), indicating the potential utilization of such nanostructures in nanocatalysis as well as sensor applications.

Acknowledgments: This work is supported by the National Science Foundation, the US Air Force Office of Scientific Research, and the US Department of Energy. The computations were performed at the National Energy Supercomputing Center at the Lawrence Berkeley Laboratory, the Army Research

Laboratory (ARL-MSRC), and the Georgia tech Center for Computational Materials Science.

REFERENCES:

(1) Landman, U.; Luedtke, W. D.; Burnham, W. A.; Colton, R. J. *Science* **1990,** *248*, 454.

(2) See review in: Agrait, N.;Yeyati, van Ruitenbeek, J.M. *Phys. Reports* **2003**, 377, 8103.

(3) R. N. Barnett, R. N.; Landman, U. *Nature* **1997**, 387, 788.

(4) Ohnishi, H.; Kondo, Y.; Takayanagi, K. *Nature* **1998**, *395*, 780.

(5) Yanson, A. I.; Rubio Bollinger, G.; van der Brom, H. E.; Agrait, N.; van Ruitenbeek, J. M. *Nature* **1998**, *395*, 783.

(6) Rodrigues, V.; Ugarte, D. *Phys. Rev. B* **2001**, *63*, 073405.

(7) Torres, J. A.; Tosatti, E.; Dal Corso, A.; Ercolessi, F.; Kohanoff, J. J.; Di Tolla, F. D.; Soler, J. M. *Surf. Sci.* **1999**, *426*, L441.

(8) Okamoto, M.; Takayanagi, K. *Phys. Rev. B* **1999**, *60*, 7808.

(9) Sanchez-Portal, D.; Artacho, E.; Junquera, J.; Ordejon, P.; Carcia, A.; Soler, J. M. *Phys. Rev. Lett.* **1999**, *83*, 3884.

(10) Häkkinen, H.; Barnett, R. N.; Scherbakov, A.; Landman, U. *J. Phys. Chem. B* **1999**, *103*, 8814.

(11) De Maria, L.; Springborg, M. *Chem. Phys. Lett.* **2000**, *323*, 293.

(12) Häkkinen, H.; Barnett, R. N.; Scherbakov, A.; Landman, U. *J. Phys. Chem. B* **2000**, *104*, 9063.

(13) Sanchez, A.; Abbet, S.; Heiz, A.U.; Schneider, W.-D.; Hakkinen, H.; Barnett, R. N.; Landman, U. J. Phys. Chem. A **1999**, 103, 9573.

(14) Häkkinen, H.; Abbet, S.; Sanchez, A.; Heiz, U.; Landman, U. *Ang. Chem. Int. Ed.* **2003**, *42*, 1297; and references therein.

(15) Hakkinen, H.; Moseler, M.; Landman, U. *Phys. Rev. Lett.* **2002**, *89*, 033401.

(16) Li, C. Z.; Sha. H.; Tao, N. J. *Phys.Rev.***1998**, *58*,6775.

(17) Li, C. Z.; He, X.; Bogozi, A.; Bunch, J. S.; Tao, N. J. *Appl. Phys. Lett.* **2000**, *76*, 1333.

(18) Bogozi, A.; Lam, O.; He, X.; Li, C. Z.; Tao, N. J.; Nagahara, L. A.; Amlani, I.; Tsui, R. *J. Am. Chem. Soc.* **2001**, *123*, 4585.

(19) Legoas, S. B.; Galvao, D. S.; Rodrigues, V.; Ugarte, D. *Phys. Rev. Lett.* **2002**, *88*, 076195.

(20) Novaes, F. D.; da Silva, A. D. R.; da Silva, E. Z.; Fazzio, A. *Phys. Rev. Lett.* **2003**, *90*, 036101.

(21) Skorodumova, N. V.; Simak, S. I. *Phys. Rev. B* **2003**, *67*, 121404.

(22) (a) Smit, R. H. M.; Noat, Y.; Untiedt, C.; Lang, N. D.; van Hemert, M.; van Ruitenbeek, J. M. Nature **2002**, *419*, 906. (b) R. H. M. Smit, Ph.D. Thesis, University of Leiden, The Netherlands, 2003. In these experiments the interaction of a hydrogen molecule with a Pt mono-atomic-wide nanowire has been studied. In addition to the vibrational frequency with hω = 64meV that is reported in (a) and attributed to shuttle motion of a bridging hydrogen molecule, a frequency above 100meV is mentioned in ((b), see section 4.6) and is attributed to a hindered rotational mode of the molecule. While the conducting electron may couple differently to various vibrational modes, both longitudinal (along the axis of the wire) and transverse ones may be measured. We also note that as stated in (a) high-energy vibrations could not be measured since the contact becomes unstable at bias voltages above 200meV.

(23) Csonka, Sz.; Halbritter, A.; Mihaly, G.; Jurdik, E.; Shklyarevskii, O. I.; Speller, S.; van Kempen, H. *Phys. Rev. Lett.* **2003**, *90*, 116803. In these experiments the physical interaction of H_2 condensed on a gold nanowire at 10-30K has been studied. The lowest peak in the measured conductance histogram at $G=0.5g_0$ is attributed, after ref. 10, to hydrogen assisted stabilization of a gold dimmer in a momo-atomic-wide wire (in ref. 10 the conductance of such dimerized bare wire was calculated as $0.58g_0$, see also fig. 2(iii)). The low temperature in these experiments may make some of the stable

configurations in our current investigation inaccessible (particularly those where a chemical rather than a physical interaction occurs), and thus differences between the measured and calculated conductances are to be expected.

(24) Garcia, Y.; Palacios, J. J.; SanFabian, E.; Verges, A.; Perez-Jimenez, A. J.; Louis, E. *Phys. Rev. B* **2004**, *69*, 41402.

(25) Barnett, R. N.; Landman, U. *Phys. Rev. B* **1993**, *48*, 2081.

(26) Perdew, J; Burk, K; Ernzerhofm M. *Phys. Rev. Lett*. **1996**, *77*, 3865.

(27) Troullier, N.; Martins, J. L., *Phys. Rev. B* **1991**, *43*, 1993.

(28) Hirose, K.; Tsukuda, M. *Phys. Rev. B* **1995**, *51*, 5278.

(29) For evaluation of the self-consistent potential used in the transfer-matrix calculation, s-local components of the Au and H atoms were used and the Kohn-Sham electronic structure was recalculated.

(30) Nakamura, Brandbyge, M.; Hansen, L. B.; Jacobsen, K. W. *Phys. Rev. Lett.* **1999**, *82*, 1538.

(31) Brandbyge, M.; Sorensen, M. R.; Jacobsen, K. W. *Phys. Rev. B* **1997**, *56*, 14956.

(32) Lian, L.; Hachet, P.; Rayner, D. M. J. Chem. Phys. **1993**, *99*, 2

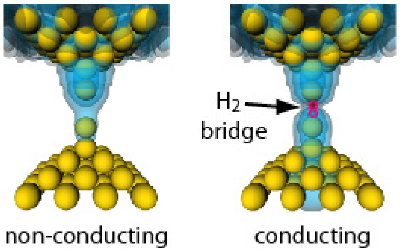

Table of Contents Graphic